POLYMER-BASED RECONSTRUCTION OF THE INFERIOR VENA CAVA IN RAT : STEM CELLS OR RGD PEPTIDE?

Margaux Pontailler[1], Eranka Illangakoon[2], Gareth R. Williams[2], Camille Marijon[1], Valérie Bellamy[1], Daniel Balvay[3], Gwenhael Autret[3], Valérie Vanneaux[4,5,6], Jérôme Larghero[4,5,6], Valérie Planat-Benard[7], Marie-Cécile Perier[8], Patrick Bruneval[8,9,10], Philippe Menasché[1,10,11], David Kalfa[1,12*]

[1]INSERM U970, PARCC & Laboratoire de Recherches Biochirurgicales, Hôpital Européen Georges Pompidou, Paris, France

[2]UCL School of Pharmacy, University College London, 29-39 Brunswick Square, London, WC1N 1AX, United Kingdom

[3]ILRI / PARCC, INSERM U 970, Hôpital Européen Georges Pompidou, Paris, France

[4]APHP, Hopital Saint-Louis, Unité de Thérapie Cellulaire, Paris, France;

[5]Univ Paris Diderot, Sorbonne Paris Cité, F-75475 Paris, France;

[6]Inserm UMR1160 et CICBT501, Institut Universitaire d'Hématologie, Hôpital Saint-Louis, Paris, France.

[7]STROMALab, UMR 5273 Université P.Sabatier, CNRS, EFS, INSERM U1031, Toulouse, France

[8]INSERM U970, PARCC, Université Paris Descartes, Sorbonne Paris Cité, Paris, France

[9]APHP, Hôpital Européen Georges Pompidou, Department of Pathology, Paris, France

[10]University Paris Descartes, Sorbonne Paris Cité, F-75475, Paris, France

[11]AP-HP, Hôpital Européen Georges Pompidou, Department of Cardiovascular Surgery, Paris, France

[12]Morgan Stanley Children's Hospital of New York, Columbia University Medical Center,

Department of Pediatric Cardiac Surgery, New York, USA; Columbia University, New York,

USA

*Corresponding author :
David Kalfa
INSERM U970, Laboratoire de Recherches Biochirurgicales,
56, Rue Leblanc, Paris 75015, France.
Tel.: +1 (347) 821-6615; fax: +33467461063.
E-mail address: davidkalfa@gmail.com

As part of a program targeted at developing a resorbable valved tube for replacement of the right ventricular outflow tract, we compared three biopolymers (polyurethane [PU], polyhydroxyalkanoate [PHBVV] and polydioxanone [PDO]) and two biofunctionalization techniques (using adipose-derived stem cells [ADSC] or the RGD peptide) in a rat model of partial inferior vena cava (IVC) replacement. Fifty-three Wistar rats first underwent partial replacement of the IVC with an acellular electrospun PDO, PU or PHBVV patch and 31 nude rats subsequently underwent the same procedure using a PDO patch biofunctionalized either by ADSC or RGD. Results were assessed both in vitro (proliferation and survival of ADSC seeded onto the different materials) and in vivo by magnetic resonance imaging (MRI), histology, immunohistochemistry [against markers of vascular cells (von Willebrand factor [vWF], smooth muscle actin [SMA]) and macrophages ([ED1 and ED2] immunostaining)] and ELISA (for the expression of various cytokines and iNOS). PDO showed the best in vitro properties. Six weeks after implantation, MRI did not detect significant luminal changes in any group. All biopolymers were evenly lined by vWF-positive cells but only PDO and PHBVV showed a continuous layer of SMA-positive cells at 3 months. PU patches resulted in a marked granulomatous inflammatory reaction. ADSC and RGD biofunctionalization yielded similar outcomes. These data confirm the good biocompatibility of PDO and support the concept that appropriately peptide-functionalized polymers may be successfully substituted for cell-loaded materials.

1. Introduction

Congenital heart diseases (CHD) occur at a prevalence of 8 to 12 per 1000 births [1] and often require reconstruction of the right ventricular outflow tract (RVOT). However, currently used devices lack regeneration and growth potential, leading to subsequent reoperations with high

morbidity and mortality [2-4]. Therefore, the development of biocompatible materials whose growth would keep pace with that of the child [5-11] still remains a clinically relevant issue.

In this setting, we have previously demonstrated the ability of a monovalved polydioxanone (PDO) patch to restore a functional RVOT in growing lambs [12]. As part of a move towards a valved tube, we have then completed this two-stage study. First, a head-to-head comparison was performed between a PDO (taken as our reference) and 2 other polymers: a polyhydroxyalkanoate (PHA) and a polyurethane (PU) which have already been used in cardiovascular research with encouraging results in terms of endothelialisation and biocompatibility [10, 11, 13-15]. In a second step, we leveraged previous findings from our laboratory [12] and others [16-18] showing that cells seeded onto polymers implanted in the circulation are rapidly cleared, and compared two functionalization modalities of the polymer patch based on cell seeding and peptide grafting, respectively. To this end, we selected adipose-derived stem cells (ADSCs) and the tripeptide Arginine-Glycine-Aspartate (RGD) with the premise that this motif, which has a long-standing efficacy record in biomaterial functionalization [19, 20], might allow scaffold repopulation from the host cells.

2. Materials & Methods

2.1. Patch fabrication

2.1.1 Materials

Polydioxanone (PDO), polyurethane (PU), 1,1,1,3,3,3-hexafluoro-2-propanol (HFIP), and chloroform were procured from Sigma-Aldrich (Gillingham, UK). Poly(3-hydroxybutyrate-

co-3-hydroxyvalerate-co-4-hydroxyvalerate) (PHBVV) was a kind gift from Bio-On SRL (Bologna, Italy), and supplied to this project as an experimental grade. RGD peptide (Ac-Gly-Arg-Cys-Gly-Arg-Gly-Asp-Ser-Pro-Gly-NH2) was provided by QGel SA (Lausanne, Switzerland).

2.1.2 Polymer processing

Solutions for electrospinning were prepared by adding the appropriate amount of polymer and peptide to the desired solvent; the resultant mixtures were stirred overnight until homogeneous solutions were obtained. The RGD-loaded polymers were prepared by directly electrospinning a mixture of PDO and RGD, thereby allowing a one-step approach for peptide incorporation. The solutions were subsequently loaded into a 5 mL syringe and a metal needle (spinneret; 0.61mm inner diameter) attached to the syringe. A high-voltage DC power supply (HCP35-35,000; FuG Elektronik, Rosenheim, Germany) was used to apply a positive voltage between the spinneret and a grounded metal collector plate (20 × 20 cm) covered in aluminium foil. The spinneret to collector distance was kept constant at 12 cm for all experiments. The polymer solution was ejected from the syringe at 1 mL / h using a syringe pump (KDS100; Cole-Parmer, London, UK). Electrospinning (ES) was carried out under ambient conditions (22 ± 3 ℃; relative humidity 35 ± 8 %). Full details of the ES parameters are given in Table 1. The production of PU and PDO fibres was highly reproducible, while the processing of the PHBVV proved to be less consistent, possibly because of the failure of using HFIP as the solvent for electrospinning this material and the subsequent switch to chloroform. The thickness of the produced patches used for the following *in vitro* and *in vivo* experiments was approximatively 350 μm.

2.1.3 Characterization

Scanning electron microscopy (SEM) was undertaken using a Quanta 200 FEG ESEM (FEI, Hillsborough, OR, USA). Samples were gold sputtered prior to examination. The images obtained were analysed using the ImageJ software (National Institutes of Health, Bethesda, MD, USA); fibre diameters were measured at over 50 locations. X-ray photoelectron spectroscopy (XPS) was performed at the NEXUS facility (Newcastle University) with the aid of a K-alpha instrument (Thermo Scientific, East Grinsted, UK) equipped with a monochromated Al Kα X-ray source. A pass energy of 40 eV and a step size of 0.1 eV were employed. Spectra were processed using the CasaXPS software (Casa Software Ltd., Teignmouth, UK).

2.2. Adipose-derived stem cell harvest, isolation and characterization

Subcutaneous inguinal adipose tissue was collected from Wistar rats under general anaesthesia by isoflurane® (AbbVie, Rungis, France) and shipped to StromaLab (Toulouse, France) for ADSC isolation according to a previously described protocol [21]. Subconfluent ADSCs were obtained after 6 days and phenotypically characterized by flow cytometry (FACSCalibur™, BD Biosciences®, Franklin Lakes, NJ, USA).

2.3. *In vitro* experimentation

ADSCs were cultivated in an alpha-MEM medium (Gibco, Carlsbad, CA, USA) supplemented with 10% FBS (Biowest, Kansas City, MO, USA), 1% antibiotic-antimycotic solution (Sigma-Aldrich, Saint Louis, MO, USA) and 0.02% b-FGF (R&D system,

Minneapolis, MN, USA). The medium was changed every 2 days. When a sufficient cell number was obtained, 1 cm ²of the PDO, PU and PHBVV patches were manually seeded with ADSCs for 48 hours at 37 ℃ under static conditions.

Cell viability on the seeded grafts was assessed by an MTT (3-[4, 5-dimethylthiazolyl-2]-2, 5-diphenyltetrazolium bromide) assay. Briefly, 1 cm ²patches were seeded with 10^5, 10^6 or 3.5×10^6 ADSCs for 48 hours in 24-well plates. Subsequently 10 µL of 5mg/mL MTT solution (Sigma-Aldrich, Saint Louis, MO, USA) for 100 µL medium were added in each well. After three hours of incubation at 37 ℃, 30 µL of isopropanol was added to each well for ten minutes. Each sample was transferred in a 96-well plate and read with a Dynex OpsysMR™ (Thermo labsystems, Milford, MA, USA) ELISA plate reader (test wavelength of 570 nm, reference wavelength of 630 nm). The acellular medium, cells killed by hydrogen peroxide, and unseeded cells were used as controls.

An additional set of PDO, PU and PHBVV patches seeded with 3.5×10^6 ADSCs for 48 hours were trypsinized (Gibco, Carlsbad, CA, USA) for 5 minutes and the cells were collected. Cell proliferation, apoptosis and necrosis were then assessed by flow cytometry using Ki67, Annexin 5 and 7 AAD (all 3 from BD Pharmingen, San Jose, CA, USA), respectively.

2.4. Study design and surgical procedures

Care of animals was in accordance with institutional guidelines. The ethical committee for animal experimentation of Paris Descartes reviewed and approved the study protocol (#13-046). A total of 84 rats were used for the study.

The study was divided into 2 parts. The first stage (n=53) consisted of the comparison of three bioabsorbable polymers, PDO, PU and PHBVV, in a Wistar female rat model (Janvier Labs SAS, Saint-Berthevin, France). The second stage (n=31) consisted of the comparison of two biofunctionalization techniques in an immunodeficient female nude rat model (Charles River, L'Arbresle, France), chosen because of the use of allogenic cells. In light of the results obtained in this initial set of experiments, the polymer selected for the biofunctionalization comparison was PDO.

All polymers were implanted as patches on the inferior vena cava (IVC) of rats. On a warming pad and under general anaesthesia by isoflurane® (AbbVie, Rungis, France), a midline laparotomy was performed. The IVC was gently occluded with microvascular clamps. A longitudinal venotomy was performed and the patch was sutured using separated 9-0 polypropylene sutures (Ethicon, Somerville, NJ, USA). After unclamping, vascular patency was visually assessed and the incision was conventionally closed in layers. The animals were then closely monitored for the occurrence of hind limb paralysis taken as a surrogate manifestation of IVC thrombosis. Animals were sacrificed by an intra-aortic injection of penthotal (Thiopenthal®, Ceva Santé Animal, Libourne, France) at 6 weeks or 3 months after patch implantation. Macroscopic patch overviews were taken with a digital camera before harvesting the patches and the surrounding IVC.

2.5. Magnetic Resonance Imaging (MRI)

Six weeks after patch implantation, MRI was performed in 11 isoflurane-anesthetized animals from each group to assess potential luminal changes such as thrombosis, stenosis or dilatation.

MRI was performed with a dedicated small-animal 4.7 Tesla MR system (Biospec 47/40 USR Bruker, Karlsruhe, Germany), using a quadrature transmit/receive body coil with a 7-cm inner diameter. The sequence of interest, a two-dimensional time-of-flight magnetic resonance angiography (2D TOF MRA), was performed to study the IVC. Axial slices were acquired from the renal vessels to the iliac bifurcation. The distance between the iliac bifurcation and the patch was measured before explantation, which allowed to identify the MRI slices corresponding to the area of patch implantation. The imaging parameters were chosen to provide bright-blood weighting whereas signal from tissue was significantly decreased : TR/TE, 18/4 ms ; $\alpha = 90°$; field of view, 7 × 5 cm; matrix, 359 × 256 ; plane resolution, 195 × 195 µm; slice thickness, 0.7 mm; interslice distance, 0.55 mm ; 3 excitations.

MRI data were analyzed using an in-house software routine in the Matlab® software (Mathworks, Natick, MA, USA). First, the vascular tree was segmented by a thresholding technique. Only bright pixels, corresponding to moving volumes of blood, were selected. Second, for each examination, the IVC was separated automatically from the aorta and other vascular structures using a strategy of contraction/expansion of the segmented vascular tree. A visual interface enabled the operator to control the segmentation with the possibility of correcting it manually. Finally, the surface of the IVC was evaluated on each slice to calculate the corresponding diameter. The native IVC was taken as the reference for diameter comparison. A 20% difference (either increase or decrease) between the diameter of the native untreated IVC and that of the patched caval segment was considered significant.

2.6. Macroscopic and histological examination

After explantation, the samples were longitudinally incised and the luminal surface of the explanted patch and the IVC were examined to detect any thrombosis. The samples were then embedded in Tissue-TeK Optimal Temperature Cutting (OCT) medium (Sakura, Torrance, CA, USA) and frozen at -180 ℃ in liquid nitrogen until they were sliced into 7-µm-thick cryosections using an ultramicrotome (LM 1850; Leica, Wetzlar, Germany). Frozen tissue sections were stained by standard hematoxylin and eosin (HES), Sirius red and alcian blue. For immunochemistry analyses, frozen tissue sections were assessed for markers of ED1 (1:100, anti-CD68) and ED2 macrophages (1:75, anti-CD163; both from AbdSerotec, Raleigh, NC, USA,). Antibody binding was detected using a biotinylated secondary antibody [1:200, anti-mouse rat absorbed IgG ; ABCYS, Les Ulis, France,] followed by the binding of an ABC/PO complex and color development with 3',3 diaminobenzidine. Nuclei were counterstained with hematoxylin. In immunofluorescence analyses, frozen tissue sections were assessed for markers of endothelial cells [von Willebrand factor (vWF), 1:200, polyclonal rabbit IgG, Dako, Glostrup, Denmark and smooth muscle cells (SMA), 1:400, clone 1A4, Sigma]. The binding of primary antibodies was detected by incubating the sections with Texas-red-conjugated anti-rabbit IgG (1:500, Alexa Fluor, Eugene, OR, USA) or FITC-conjugated anti-mouse IgG (1:300, Vector, Burlingame, CA, USA) antibodies. Nuclear counterstaining was performed with 4',6-diamidino-2-phenylindole. Frozen tissue sections from both Wistar and nude rat IVC served as controls. All samples were analyzed with a microscope (Leica DMIL, Wetzlar, Germany) equipped with a digital camera (Qicam; Qimaging, Burnaby, BC, Canada) at 20× magnification. Digital images were then processed with the Metamorph® software (Universal Imaging Corporation, Downington, PA, USA). vWF and SMA results are expressed as a ratio between the endoluminal surface occupied by vWF- or SMA-positive cells and that of the whole patch. ED1 and ED2 results are expressed

as a ratio between the surface occupied by ED1- or ED2-positive cells and that of the whole patch.

2.7. ELISA tests

The explanted patches were separated from the native IVC and dissolved in a Tri-Reagent solution (Sigma®) for protein extraction during 24 hours before ELISA testing. Rat Monocyte-Chemoattractant Protein-1 (MCP-1), Interleukin-6 (IL-6) and Interleukin-10 (IL-10) ELISA kits (RayBio®, Norcross, GA, USA) and rat inducible NO Synthase (iNOS) ELISA kit (SunRedBio®, Shangai, China) were used per manufacturer's protocols. The results were read in a Dynex OpsysMR (ThermoLabsystems®, Vienna, VA, USA) ELISA plate reader (450 nm wavelength).

2.8. Statistical analysis

All values are expressed as mean ± standard deviation for continuous variables and n (%) for categorical variables. Comparisons between the 3 biopolymers were performed using analysis of variance or analysis of variance on ranks (when appropriate) for quantitative variables and using an exact Fisher test for qualitative variables. Multiple comparisons were done using pairwise comparison with Tukey correction for post-hoc tests. Comparisons between the 2 biofunctionalization techniques were performed using Student test or Wilcoxon Mann-Whitney test when appropriate. For all analyses, a two-tailed p-value <0.05 was considered statistically significant. Statistical analyses were performed by an independent statistician blinded to the treatment group, using the SAS 9.2 software (Statistical Analysis System, Cary, NC, USA).

3. Results

3.1. Electrospun patch fabrication and characterization

SEM images of the PDO, PU, and PHBVV fibres are shown in Figure 1. In all cases, the materials produced consisted of intertwined meshes of one-dimensional fibre strands. The mats were observed to be porous, with maximum pore sizes of ca. 1 – 2 μm. The fibres were generally linear and had smooth surfaces. The PU materials appeared "flattened", while the PHBVV materials showed evidence for some "bead-on-string" type morphology, likely related to the difficulties in optimizing electrospinning of this polymer. Fibre diameters and the porosity are detailed in Table 2.

To confirm the successful incorporation of the peptide into the PDO-RGD fibres, X-ray photoelectron spectroscopy (XPS) was used to probe the fibre surface composition. The spectra clearly show the presence of N atoms; these can only come from the RGD peptide, thereby demonstrating that peptide is displayed at the surface of the fibres. From three independent measurements, the surface composition (as weight %) is calculated to be C: 56.8 ± 0.91 %; O: 40.8 ± 0.72 %; N: 2.38 ± 0.24 %. From the ratio at which the starting materials were combined, the bulk fibres should comprise C: 46.8 %; O: 46.7 %; N: 0.46 %; S: 0.064 %. This therefore indicates that there is some sequestration of peptide to the fibre surfaces (the observed N content is ca. 5-fold greater than that calculated for the bulk).

3.2. *In vitro* assessment

Cultivated ADSCs expressed CD44 and CD90, were negative for CD45 and were able to differentiate into adipocytes and osteoblasts in response to the appropriate cues (Oil-Red-O and Alizarin red, respectively). On the basis of the MTT assay, the viability of ADSC was greater on PDO than on PHBVV and PU patches (global p-value < 0.0001; Fig. 2). Flow cytometry revealed that ADSCs had high proliferation rates (PDO: 55% ; PHBVV: 64% ; PU: 55%) and low apoptosis and death rates (PDO: 1.25% (apoptosis) and 1.2% (death) ; PHBVV: 3.2% and 5.4% ; PU: 5.65% and 2.2% ; Fig. 3).

3.3. *In vivo* polymer comparison

Fifty-three female Wistar rats underwent a partial replacement of the IVC with an acellular electrospun PDO (n=18), PU (n=21) or PHBVV (n=14) patch. None of them displayed any postoperative paralysis. Eleven rats in each group underwent MRI imaging at 6 weeks, which showed no stenosis, thrombosis or aneurysm in the area of the patch implantation (Fig. 4). Forty-four rats were sacrificed at 6 weeks and 3 rats of each group at 3 months. Macroscopically, there was no thrombosis on the endoluminal surface of any of the 3 polymers tested. At 3 months, the PDO patches could no longer be detected and distinguished from the native IVC, whereas the PHBVV patches were not as completely integrated (Fig. 5(a) and (b)). In the PU group, granulomas were found in 4 (22%) of the 18 patches at 6 weeks, and in all specimens at 3 months (Fig. 5(c)). Figures 6 and 7 (a, f, k) show the different degradation rates of the biopolymers.

Histological and ELISA results at 6 weeks and 3 months are summarized in Tables 3 and 4, respectively. Hematoxylin/Eosin staining reveals that the cells were able to penetrate the whole thickness of the PDO (loaded with RGD or not) and PHBVV patches, whereas they were only found surrounding the PU patches, either at 6 weeks or 3 months (Figs 6 and 7. [a,

f, k]). The 3 polymeric patches were evenly lined by vWF-positive cells at 6 weeks and 3 months (Figs. 6 and 7(b), (g) and (l)). The number of SMA-positive cells was higher on PDO and PHBVV patches than on PU patches ($p = 0.006$ and $p = 0.0173$, respectively, at 6 weeks; Figs. 6 and 7 (c) , (h) , and (m)). Inflammatory cells were found surrounding the PU patches, whereas they infiltrated the PDO and PHBVV ones (Figs. 6 and 7. (d), (e), (i), (j), (n), and (o)). The infiltration of pro-inflammatory ED1 macrophages was lower in the PHBVV group than in the PDO ($p = 0.0084$) and PU ($p = 0.0066$) groups at 6 weeks. At 3 months, ED1 infiltration had markedly decreased compared to the 6-week time point in the PDO and PHBVV patches (-80% and -33%, respectively) whereas it remained stable and high in the PU group (92% at 6 weeks and 83% at 3 months). ED2 regulatory macrophages and the ED2/ED1 ratio were higher in the PU group at 6 weeks. At 3 months, ED2/ED1 ratios had increased in the PDO and PHBVV groups (+45% and +7%, respectively, compared to 6 weeks), and decreased in the PU group (-16%). The latter polymer yielded the lowest ratio of regulatory macrophages relative to the total macrophage pool (ED2/ED1 = 56 ± 6 %, versus 64 ± 31 % for PHBVV and 100% for PDO). Three months after implantation, there was evidence for an extracellular matrix synthesis of varying extent and pattern in the three biopolymer-treated groups (Fig. 8). PDO was associated with the greatest collagen and glycosaminoglycans density in a well organised extracellular matrix, resembling that of the native IVC composition, followed by PHBVV (Fig. 8(a,b,e,f)). Extracellular matrix in contact of the PU appeared to be less developed and less organized (Fig. 8 (c,d)).

At 6 weeks, explanted patches of PHBVV and PDO showed higher concentrations of IL-6 than PU ($p = 0.0002$ and $p < 0.0001$ respectively). IL-6 was further upregulated in each group at 3 months compared to 6 weeks (PDO : +42% ; PU : +57% ; PHBVV : +98%). At 6 weeks, PDO showed higher concentrations of MCP-1 compared to PHBVV and PU ($p < 0.0001$ and

p = 0.0007, respectively); however, at 3 months values had decreased in all 3 groups (PDO : -40% ; PU : -14% ; PHBVV : -17%). There were no significant differences in iNOS concentrations between the 3 biopolymer patches (p = 0.90). The expression of the anti-inflammatory IL-10 cytokine was highest in the PDO group at 6 weeks (global p-value = 0.015). IL-10 production was then stable in the PDO and PU groups, whereas its expression nearly doubled in the PHBVV group (+94%) between 6 weeks and 3 months.

3.4. Biofunctionalization techniques comparison

Thirty-one immunodeficient nude rats underwent an IVC partial replacement by either a PDO patch seeded with ADSC (n=17) or a PDO patch biofunctionalized by RGD (n=14). MRI imaging at 6 weeks failed to detect thrombosis or stenosis in the patch implantation area. No granulomas or thrombosis were found during the macroscopic analyses. At 6 weeks, the biofunctionnalized patches were well integrated to the native IVC wall and their luminal surfaces were evenly lined with continuous layers of endothelial (Fig. 9 (b), and (g)) and smooth muscle cells (Fig. 9 (c), and (h)). ED1 macrophage infiltration was more pronounced in ADSC-biofunctionalized patches (p = 0.049; Fig. 9. (d), and (i)) whereas ED2 regulatory macrophage infiltration was similar in both groups (Fig. 9. (e), and (j)). ELISA measurements of IL-6, IL-10, iNOS and MCP-1 showed no statistical differences between ADSC and RGD biofunctionalization. The histological and ELISA results at 6 weeks are summarized in Table 5.

At 3 months, the cell and peptide-biofunctionalized patches had disappeared and were fully integrated in the native IVC wall. There were no statistical differences between the two biofunctionalization techniques with regard to histological and ELISA end points (Fig. 10 and

Table 6). In comparison to the 6-week data, there was a decrease in the number of ED1 macrophages and an increase of ED2 regulatory macrophages in both groups. There was also evidence for a well organized extracellular matrix, similar to that of the native IVC, with no difference between the two biofunctionalized polymers (Fig. 11). IL-6, MCP-1 and iNOS expression was further upregulated at 3 months in both groups compared to the 6 weeks, whereas IL-10 concentrations remained stable.

4. Discussion

Several materials have been tested clinically for reconstructing the RVOT [22-29] but their common limitation is the lack of a growth potential which leads to reoperations, with their attendant risk of increased morbidity and mortality.

In an attempt to address this issue, we have undertaken a program aimed at developing a degradable valved polymeric tube designed to harness endogenous healing mechanisms to achieve the full replacement of the device by an autologous living conduit. Initial proof-of-principle experiments entailing the placement of a mesenchymal stem cell-seeded PDO monocusp patch across the pulmonary annulus in growing lambs confirmed the high biocompatibility of this polymer which, over time, was replaced by a host-derived tissue histologically similar to the native pulmonary arterial wall [12]. This result is consistent with the successful outcomes yielded by PDO valvular rings implanted in children [30]. However, a drawback of PDO in our experiments was its fast degradation which led us to compare it, in a head-to-head fashion, with two other polymers (PU and PHBVV). All three materials were selected for their alleged biocompatibility, mechanical properties, suitability for electrospinning-based manufacturing, and possibility of regulatory approvability for human use. Although some teams have made replacements of the RVOT in rats [31], we found

partial replacement of the rat IVC, which shares with the pulmonary artery low-pressure patterns, a more suitable model for screening experiments.

In our study, the 3 different acellular electrospun patches displayed complete in vivo endothelialisation at 6 weeks and 2 of them, PDO and PHBVV, featured a continuous layer of smooth muscle cells at 3 months. We assume that self-endothelialisation and neo-vessel regeneration were obtained by both recruitment of circulating progenitor cells and migration from the edges of the native vessel [32]. Although we did not investigate endothelial cell function, the latter was likely adequate since no thrombosis was found either macroscopically or microscopically. Overall, our results are in line with those of Matsumara et al. who evaluated cell-free scaffolds in the IVC and pulmonary valve locations in dogs and found endothelialisation, vascular smooth muscle cell proliferation and synthesis of an extra-cellular matrix [33,34].

Such remodelling of the matrix is a key process in vascular restoration and is impacted by the number and polarity of invading monocytes and macrophages. From this standpoint, PDO and PHVBB outperformed PU with regard to the predominance of infiltrating regulatory ED2 macrophages, a phenotype associated with less inflammatory tissue scarring and improved remodelling [35, 36]. The enhanced ED2 response to PDO and PHBVV is consistent with our concurrent finding of higher expressions of the anti-inflammatory IL-10 cytokine and of the MCP-1 chemokine. In contrast, PU was associated with a much greater inflammatory response, with a persisting insulation of the patches and, occasionally, granulomas, which have also been reported in other applications [37, 38]. Whether a physico-chemically different PU might more favourably affect host tissue responses will be the subject of future investigations.

Another important finding from the previous work of our laboratory and others [12, 16-18] is that polymer-seeded cells are cleared over time which leads to speculate that the grafted cells do not structurally integrate within the neo-vessel wall, but rather act as platforms releasing signalling molecules that may recruit host cells. This hypothesis provides a robust rationale for testing whether cells can thus be replaced by biomimetic compounds which could duplicate their recruiting effects and promote self-healing. Indeed, the use of different bioactive peptides as substitutes for cell therapy has been successfully tested in cardiac regeneration and other specialties [17, 39-42].

In the present study, we selected RGD, a tri-peptide composed of Arginine-Glycine-Aspartate that mimics the integrin binding site of cells and the extra-cellular matrix [43] and has already been successfully tested as a biofunctionalization motif [44]. Grafting of RGD on a polymer was compared, again in a head-to-head fashion, with ADSC selected because of their ease of procurement, richness of their secretome and potential for human applications. PDO was chosen as the material common to these two biologics because it had yielded the most encouraging signals in the first set of experiments and with the recognition that its above mentioned fast degradation kinetics were not a definite limiting factor in that it could be addressed by altering density of the fibre network through fine-tuned electrospinning settings, or by combining it with another polymer featuring superior mechanical properties.

No significant differences were found between RGD and ADSC in terms of vascular remodeling, neo-vessel formation, inflammatory cell response and cytokine secretion. This result is consistent with that reported by Roh et al. [17] who showed, in a murine model of infrarenal IVC replacement, that the restorative patterns observed after implantation of a human bone marrow mononuclear cell seeded polymer could be duplicated by replacing cells with MCP-1 grafting on the scaffold. We acknowledge, however, that in the absence of

covalent binding, the PDO can dissolve from the surface of the polymer with the possibility that its soluble form may, at the opposite of our objective, act as an integrin blocker preventing cell adhesion [45-46]. Thus, while the method used in this study for immobilizing RGD in the scaffold does not allow to conclusively establish that the tripeptide actually contributed to recruit host cells, the slow degradation rate of PDO may still have permitted RGD embedded into the network to remain active with regard to cell homing during a prolonged period of time while the outer fibres were being dissolved.

Altogether, these data reinforce the idea that engineering of polymeric scaffolds might allow to skip seeding of cells, provided the scaffolds are functionalized with bioactive peptides able to enhance host cell homing to generate a native-like tissue. Should such a concept be confirmed in clinically relevant large animal models, it could dramatically streamline the translational process and open clinically relevant perspectives for the RVOT replacement in children suffering from congenital cardiac abnormalities. .

5. Acknowledgements

This work was funded by grants from the Agence de la Biomédecine (Biogreffe) and by the LeDucq Foundation (SHAPEHEART network). The authors thank the Fonds d'Etudes et de Recherche du Corps Médical des Hôpitaux de Paris for its support. The authors thank Bio-On SRL for the kind gift of PHBVV, QGel for providing the RGD and the EPSRC for access to the UK National EPSRC XPS User Service (NEXUS) at Newcastle University. We also thank Dr Naoko Sano for performing XPS measurements, and Mr David McCarthy for recording SEM images.

6. Author Disclosure Statement

No competing financial interests exist.

7. References

[1] Dolk H, Loane M, EUROCAT Steering Committee: Congenital heart defects in Europe: 2000-2005. Newtownabbey, Northern Ireland: University of Ulster; March 2009. Available at: http://www.eurocat-network.eu/content/EUROCAT-Special-Report-CHD.pdf

[2] Dearani JA, Danielson GK, Puga FJ, Schaff HV, Warnes CW, Driscoll DJ, Schleck CD, Ilstrup DM. Late follow-up of 1095 patients undergoing operation for complex congenital heart disease utilizing pulmonary ventricle to pulmonary artery conduits. Ann Thorac Surg **75**, 399, 2003.

[3] Christenson JT, Sierra J, Colina Manzano NE, Jolou J, Beghetti M, Kalangos A. Homografts and xenografts for right ventricular outflow tract reconstruction: long-term results. Ann Thorac Surg **90**, 1287, 2010.

[4] Poynter JA, Eghtesady P, McCrindle BW, Walters HL 3rd, Kirshbom PM, Blackstone EH, Husain SA, Overman DM, Austin EH, Karamlou T, Lodge AJ, St Louis JD, Gruber PJ, Ziemer G, Davies RR, Jacobs JP, Brown JW, Williams WG, Tchervenkov CI, Jacobs ML, Caldarone CA; Congenital Heart Surgeons' Society. Association of pulmonary conduit type and size with durability in infants and young children. Ann Thorac Surg **96**, 1695, 2013.

[5] Dohmen PM, Lembcke A, Holinski S, Pruss A, Konertz W. Ten years of clinical results with a tissue-engineered pulmonary valve. Ann Thorac Surg **92**, 1308, 2011.

[6] Cho SW, Park HJ, Ryu JH, Kim SH, Kim YH, Choi CY, Lee MJ, Kim JS, Jang IS, Kim DI, Kim BS. Vascular patches tissue-engineered with autologous bone marrow-derived cells and decellularized tissue matrices. Biomaterials **26**, 1915, 2005.

[7] Hoerstrup SP, Kadner A, Breymann C, Maurus CF, Guenter CI, Sodian R, Visjager JF, Zund G, Turina MI. Living, autologous pulmonary artery conduits tissue engineered from human umbilical cord cells. Ann Thorac Surg **74**, 46, 2002.

[8] Hoerstrup SP, Kadner A, Melnitchouk S, Trojan A, Eid K, Tracy J, Sodian R, Visjager JF, Kolb SA, Grunenfelder J, Zund G, Turina MI. Tissue engineering of functional trileaflet heart valves from human marrow stromal cells. Circulation **106 Suppl**, 143, 2002.

[9] Kelm JM, Emmert MY, Zürcher A, Schmidt D, Begus Nahrmann Y, Rudolph KL, Weber B, Brokopp CE, Frauenfelder T, Leschka S, Odermatt B, Jenni R, Falk V, Zünd G, Hoerstrup SP. Functionality, growth and accelerated aging of tissue engineered living autologous vascular grafts. Biomaterials **33**, 8277, 2012.

[10] Sodian R, Lueders C, Kraemer L, Kuebler W, Shakibaei M, Reichart B, Daebritz S, Hetzer R. Tissue engineering of autologous human heart valves using cryopreserved vascular umbilical cord cells. Ann Thorac Surg **81**, 2207, 2006.

[11] Fujimoto KL, Guan J, Oshima H, Sakai T, Wagner WR. In Vivo Evaluation of a Porous, Elastic, Biodegradable Patch for Reconstructive Cardiac Procedures. Ann Thorac Surg **83**, 648, 2007.

[12] Kalfa D, Bel A, Chen-Tournoux A, Della Martina A, Rochereau P, Coz C, Bellamy V, Bensalah M, Vanneaux V, Lecourt S, Mousseaux E, Bruneval P, Larghero J, Menasché P. A polydioxanone electrospun valved patch to replace the right ventricular outflow tract in a growing lamb model. Biomaterials **31**, 4056, 2010.

[13] Sodian R, Hoerstrup SP, Sperling JS, Daebritz S, Martin DP, Moran AM, Kim BS, Schoen FJ, Vacanti JP, Mayer JE Jr. Early in vivo experience with tissue-engineered trileaflet heart valves. Circulation **102 Suppl** 22, 2000.

[14] Guelcher SA. Biodegradable polyurethanes: synthesis and applications in regenerative medicine. Tissue Eng Part B Rev **14**, 3, 2008.

[15] Siepe M, Giraud MN, Liljensten E, Nydegger U, Menasche P, Carrel T, Tevaearai HT. Construction of Skeletal Myoblast-Based Polyurethane Scaffolds for Myocardial Repair. Artif Organs **31**, 425, 2007.

[16] O'Neill TJ 4th, Wamhoff BR, Owens GK, Skalak TC. Mobilization of bone marrow-derived cells enhances the angiogenic response to hypoxia without transdifferentiation into endothelial cells. Circ Res **97**, 1027, 2005.

[17] Roh JD, Sawh-Martinez R, Brennan MP, Jay SM, Devine L, Rao DA, Yi T, Mirensky TL, Nalbandian A, Udelsman B, Hibino N, Shinoka T, Saltzman WM, Snyder E, Kyriakides TR, Pober JS, Breuer CK. Tissue-engineered vascular grafts transform into mature blood vessels via an inflammation-mediated process of vascular remodeling. Proc Natl Acad Sci U S A **107**, 4669, 2010.

[18] Kurobe H, Maxfield MW, Breuer CK, Shinoka T. Concise review: tissue-engineered vascular grafts for cardiac surgery: past, present, and future. Stem Cells Transl Med **1**, 566, 2012.

[19] Hersel U, Dahmen C, Kessler H. RGD modified polymers: biomaterials for stimulated cell adhesion and beyond. Biomaterials **24**, 4385, 2003.

[20] Elbert DL and Hubbell JA. Conjugate addition reactions combined with free-radical cross-linking for the design of materials for tissue engineering. Biomacromolecules **2**, 430, 2001.

[21] Hamdi H, Planat-Benard VE, Bel A, Neamatalla H, Saccenti L, Calderon D, Bellamy V, Bon M, Perrier MC, Mandet C, Bruneval P, Casteilla L, Hagège AA, Pucéat M, Agbulut O, Menasché P. Long Term Functional Benefits of Epicardial patches as Cell Carriers. Cell Transplant **23**, 87, 2014.

[22] Liu XG, Wu KH, Li XF, Shi C, Wang ZY, Tang Z, Shi XQ, Liu YL. Simultaneous enlargement of the pulmonary annulus and the pulmonary cusp with autologous pericardium in right ventricular outflow tract reconstruction. J Surg Res **136**, 320, 2006.

[23]Sasson L, Houri S, Raucher Sternfeld A, Cohen I, Lenczner O, Bove EL, Kapusta L, Tamir A. Right ventricular outflow tract strategies for repair of tetralogy of Fallot: effect of monocusp valve reconstruction. Eur J Cardiothorac Surg **43**, 743, 2013.

[24] Moore CH, Martelli V, Ross DN. Reconstruction of right ventricular outflow tract with a valved conduit in 75 cases of congenital heart disease. J Thorac Cardiovasc Surg **71**, 11, 1976.

[25] Brown JW, Ruzmetov M, Rodefeld MD, Vijay P, Darragh RK. Valved bovine jugular vein conduits for right ventricular outflow tract reconstruction in children: an attractive alternative to pulmonary homograft. Ann Thorac Surg **82**, 909, 2006.

[26] Holmes AA, Co S, Human DG, Leblanc JG, Campbell AI. The Contegra conduit: Late outcomes in right ventricular outflow tract reconstruction. Ann Pediatr Cardiol **5**, 27, 2012.

[27] Belli E, Salihoğlu E, Leobon B, Roubertie F, Ly M, Roussin R, Serraf A. The performance of Hancock porcine-valved Dacron conduit for right ventricular outflow tract reconstruction. Ann Thorac Surg **89**, 152, 2010.

[28] Dos L, Muñoz-Guijosa C, Mendez AB, Ginel A, Montiel J, Padro JM, Subirana MT. Long term outcome of mechanical valve prosthesis in the pulmonary position. Int J Cardiol **150**, 173, 2011.

[29] Lee YS, Lee HD. Percutaneous pulmonary valve implantation. Korean Circ J **42**, 652, 2012.

[30] Kalangos A, Christenson JT, Beghetti M, Cikirikcioglu M, Kamentsidis D, Aggoun Y. Mitral valve repair for rheumatic valve disease in children: midterm results and impact of the use of a biodegradable mitral ring. Ann Thorac Surg **86**, 161, 2008.

[31] Sakai T, Li RK, Weisel RD, Mickle DA, Kim ET, Jia ZQ, Yau TM. The fate of a tissue-engineered cardiac graft in the right ventricular outflow tract of the rat. J Thorac Cardiovasc Surg **121**, 932, 2001.

[32] Xu Q, Zhang Z, Davison F, Hu Y. Circulating progenitor cells regenerate endothelium of vein graft atherosclerosis, which is diminished in ApoE-deficient mice. Circ Res **93**, 76, 2003.

[33] Matsumura G, Nitta N, Matsuda S, Sakamoto Y, Isayama N, Yamazaki K, Ikada Y. Long-term results of cell-free biodegradable scaffolds for in situ tissue-engineering vasculature: in a canine inferior vena cava model. PLoS One **7**, e35760, 2012.

[34] Matsumura G, Isayama N, Matsuda S, Taki K, Sakamoto Y, Ikada Y, Yamazaki K. Long-term results of cell-free biodegradable scaffolds for in situ tissue engineering of pulmonary artery in a canine model. Biomaterials **34**, 6422, 2013.

[35] Brown BN, Valentin JE, Stewart-Akers AM, McCabe GP, Badylak SF. Macrophage phenotype and remodeling outcomes in response to biologic scaffolds with and without a cellular component. Biomaterials **30**, 1482, 2009.

[36] Brown BN, Londono R, Tottey S, Zhang L, Kukla KA, Wolf MT, Daly KA, Reing JE, Badylak SF. Macrophage phenotype as a predictor of constructive remodeling following the implantation of biologically derived surgical mesh materials. Acta Biomater **8**, 978, 2012.

[37] Lee JH, Kang MS and Yang JW. Clinicopathologic findings after nasolacrimal polyurethane stent implantations. Korean J Ophthalmol **19**, 252, 2005.

[38] Bassetto F, Scarpa C, Caccialanza E, Montesco MC, Magnani P. Histological features of periprosthetic mammary capsules: silicone vs. polyurethane. Aesthetic Plast Surg **34**, 481, 2010.

[39] Yin H, Gao M, Leoni L, Han H, Zhang X, Fu Z. The therapeutic role of monocyte chemoattractant protein-1 in a renal tissue engineering strategy for diabetic patients. PLoS One **8**, e57635, 2013.

[40] Suzuki T, Lee CH, Chen M, Zhao W, Fu SY, Qi JJ, Chotkowski G, Eisig SB, Wong A, Mao JJ. Induced migration of dental pulp stem cells for in vivo pulp regeneration. J Dent Res **90**, 1013, 2011.

[41] Vadal àG, Mozetic P, Rainer A, Centola M, Loppini M, Trombetta M, Denaro V. Bioactive electrospun scaffold for annulus fibrosus repair and regeneration. Eur Spine J **21 Suppl**, 20, 2012.

[42] Prokoph S, Chavakis E, Levental KR, Zieris A, Freudenberg U, Dimmeler S, Werner C. Sustained delivery of SDF-1α from heparin-based hydrogels to attract circulating pro-angiogenic cells. Biomaterials **33**, 4792, 2012.

[43] Ruoslahti E, Pierschbacher MD. New perspectives in cell adhesion: RGD and integrins. Science **238**, 491 1987.

[44] Lin YS, Wang SS, Chung TW, Wang YH, Chiou SH, Hsu JJ, Chou NK, Hsieh KH, Chu SH. Growth of endothelial cells on different concentrations of Gly-Arg-Gly-Asp photochemically grafted in polyethylene glycol modified polyurethane. Artif Organs **25**, 617, 2001.

[45] Shabbir SH, Eisenberg JL, Mrksich M. An inhibitor of a cell adhesion receptor stimulates cell migration. Angew Chem Int Ed Engl. 2010 Oct 11;**49**(42):7706-9.

[46] Patra C, Talukdar S, Novoyatleva T, Velagala SR, Mühlfeld C, Kundu B, Kundu SC, Engel FB. Silk protein fibroin from Antheraea mylitta for cardiac tissue engineering. Biomaterials. 2012 Mar;**33**(9):2673-80.

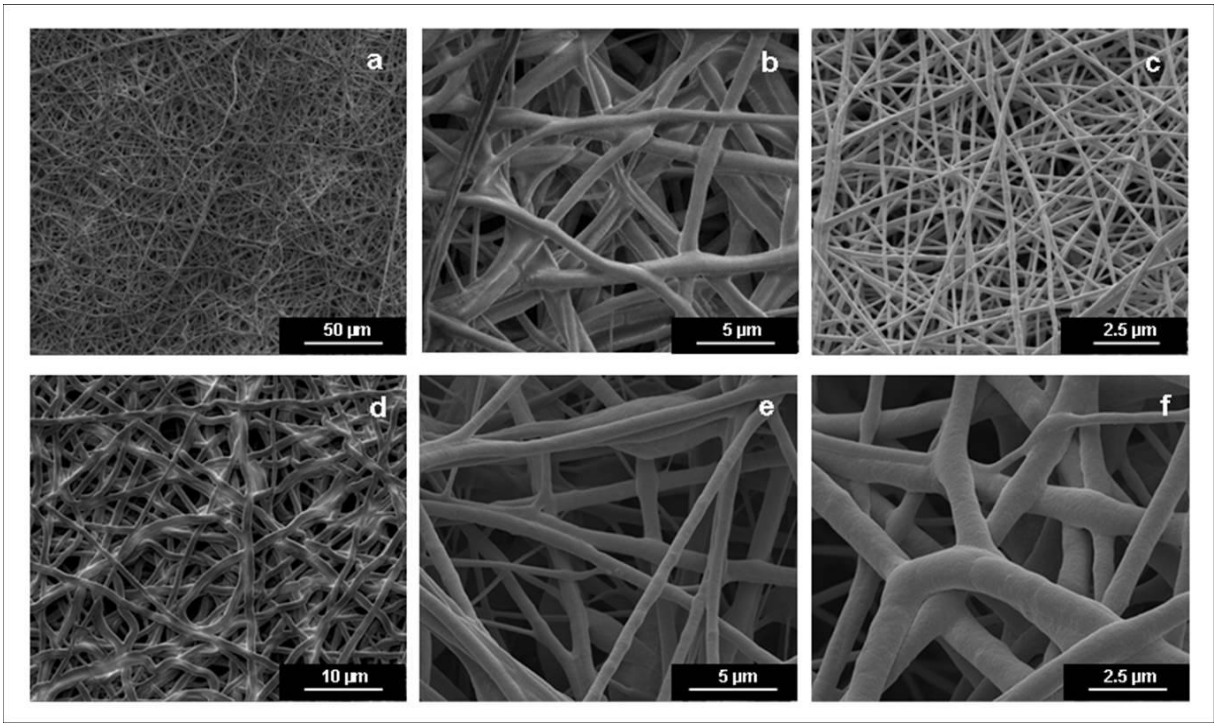

Figure 1: SEM images of the electrospun fibre mats. (a, b) PDO fibres; (c) PDO-RGD fibres; (d) PU fibres; (e, f) PHBVV fibres. (applied voltage : 2.0 kV for PDO; 5.0 kV for PDO-RGD, PU and PHBVV)

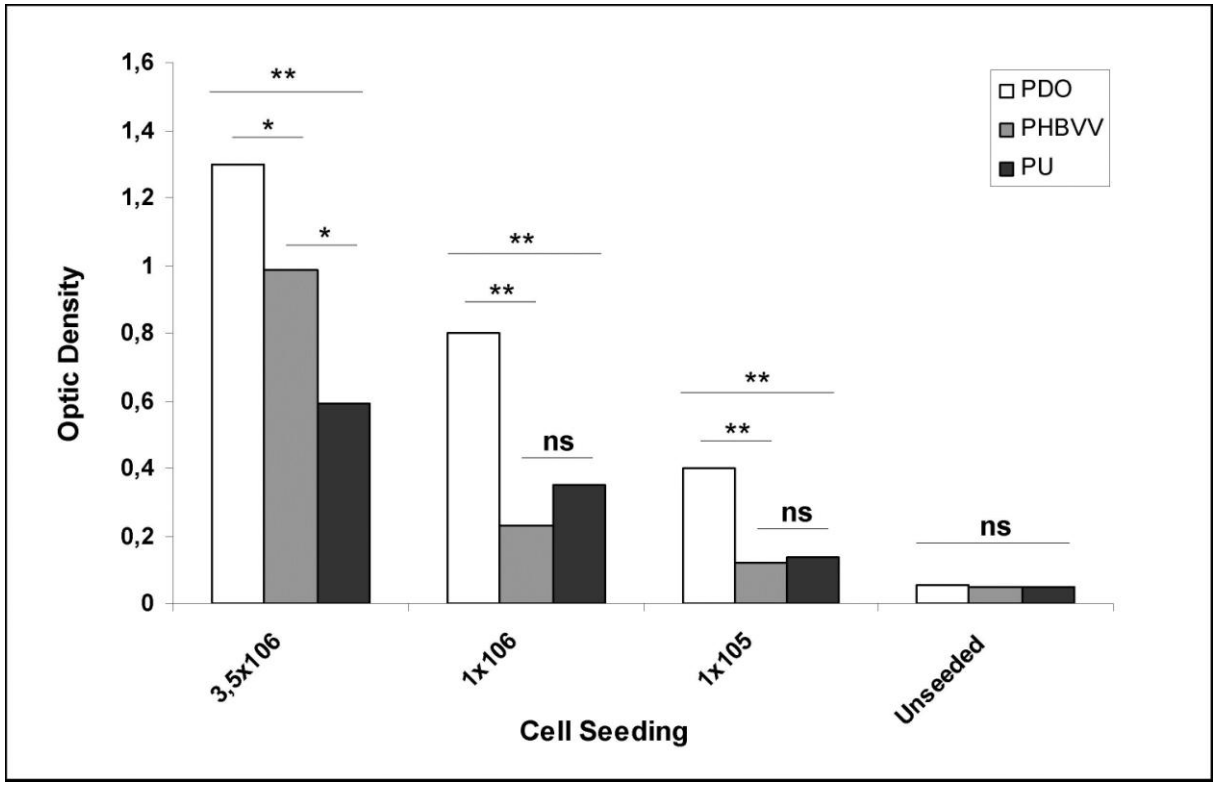

Figure 2. MTT assay results. PDO shows the best in vitro properties with a significantly higher cell viability after seeding than the other materials. With a 3,5 $\times 10^6$ ADSC cell seeding, cell viability with PDO is significantly higher than that in PHBVV (PHBVV: 0.99 $\pm$0.13 and PDO: 1. 30 $\pm$0.25 ; $p < 0.046$). Both cell viabilities in PDO and PHBVV are higher than in the PU group (0.59 $\pm$0.15 ; $p < 0.0001$ and $p < 0.0089$, respectively). (Data were compared by analysis of variance and pairwise comparison with Tukey correction for multiple comparisons ; * $p < 0.05$; ** $p < 0.0001$; ns, not significant.)

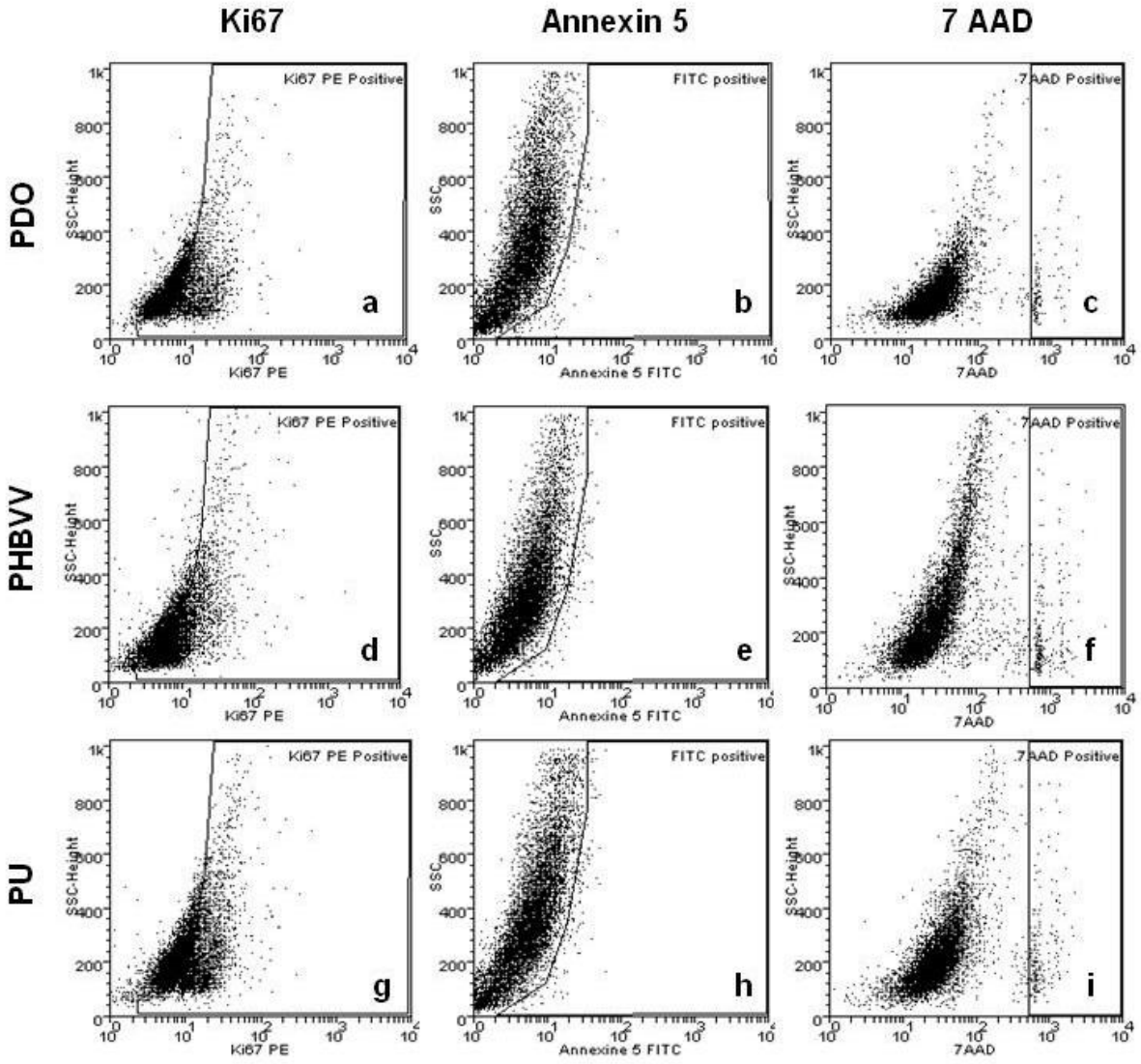

Figure 3. Flow cytometry data for the polymer patches. ADSC seeded on PDO, PHA & PU exhibit high proliferation (a,d,g) and low apoptosis and necrosis (b,e,h ; c,f,i) rates.

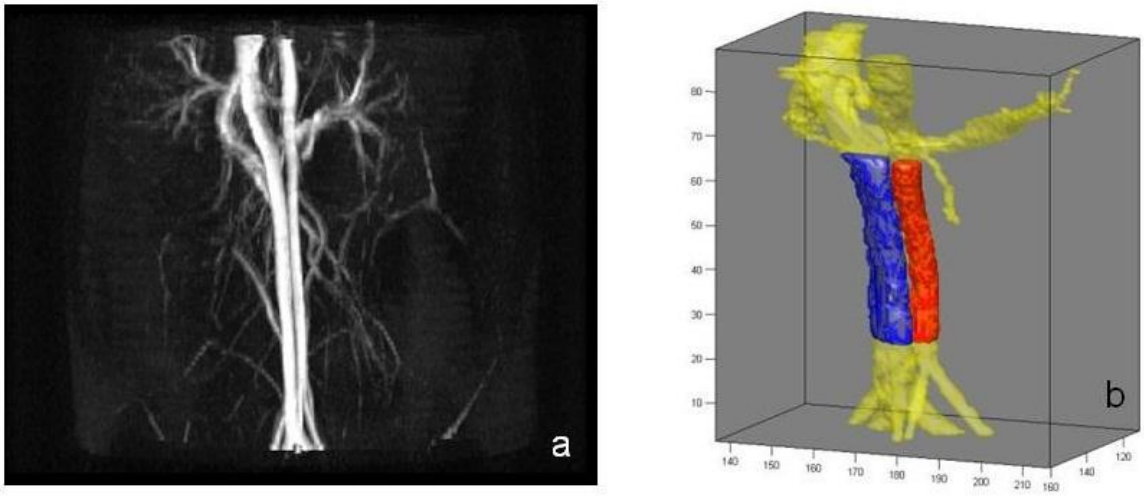

Figure 4. MRI Imaging (a) and reconstruction (b). Example of a PDO patch implanted on the IVC of a Wistar rat. No thrombosis, stenosis or dilatation was found in any rat investigated in this study.

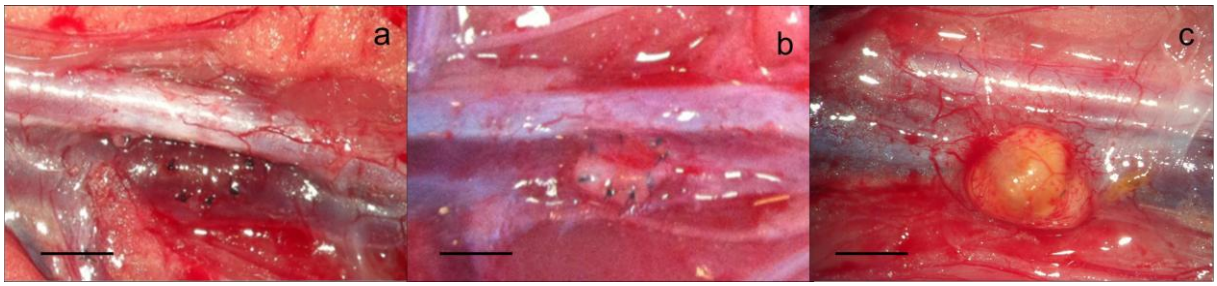

Figure 5. Macroscopic views of the implanted patches at 3 months. All grafted vessels were patent at 3 months post-implantation. The PDO patch is completely integrated in the IVC wall (a) whereas the PHBVV patch can still be distinguished from the IVC (b). A granuloma surrounds the PU patch (c). (scale bar : 3mm)

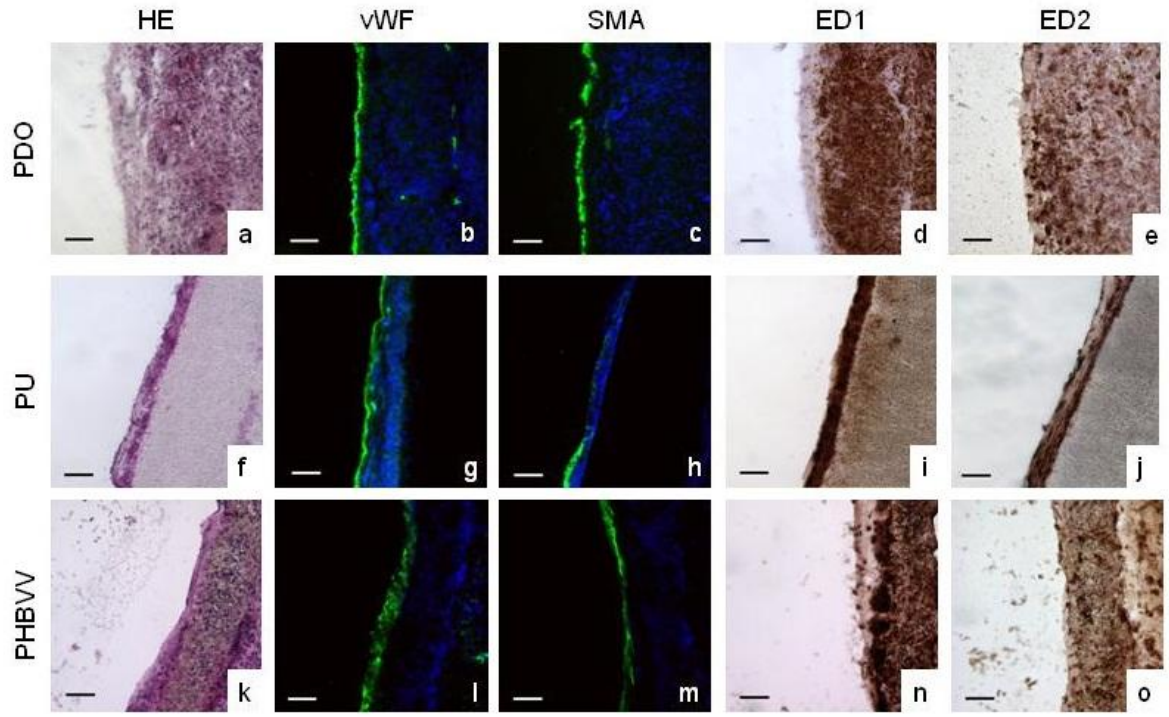

Figure 6. Analysis of the biopolymer patches explanted after 6 weeks. All biopolymers are evenly lined with endothelial cells (b, g, l). The number of SMA-positive cells is higher on PDO and PHBVV patches in comparison with the PU patches (c, h, m). PU patches are insulated by macrophages (i, j) whereas inflammatory cells infiltrate both PDO (d,e) and PHBVV patches (n,o). DAPI staining shows a greater cellularisation of the PDO and PHBVV patches compared with PU (b,c,g,h,l,m). Scale bar : 50 µm.

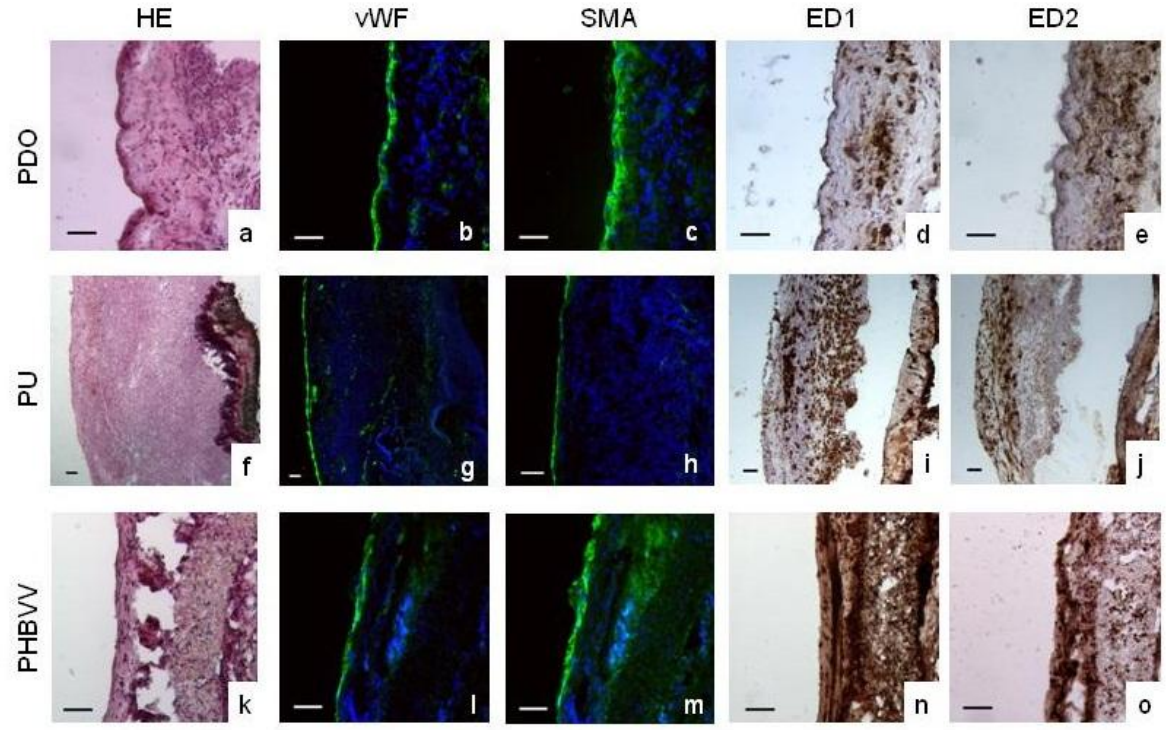

Figure 7. Analysis of the biopolymer patches explanted after 3 months. All biopolymers are evenly lined with endothelial (b,g,l) and smooth muscle cells (c,h,m). PDO has totally disappeared and is replaced by a neo-tissue similar to the native IVC (a-e). PU is encapsulated in a granulomatous inflammatory reaction (i,j). PHBVV starts to be degraded (n,o). DAPI staining again shows a greater cellularisation of the PDO and PHBVV patches compared with PU (b,c,g,h,l,m). Scale bar : 50 µm.

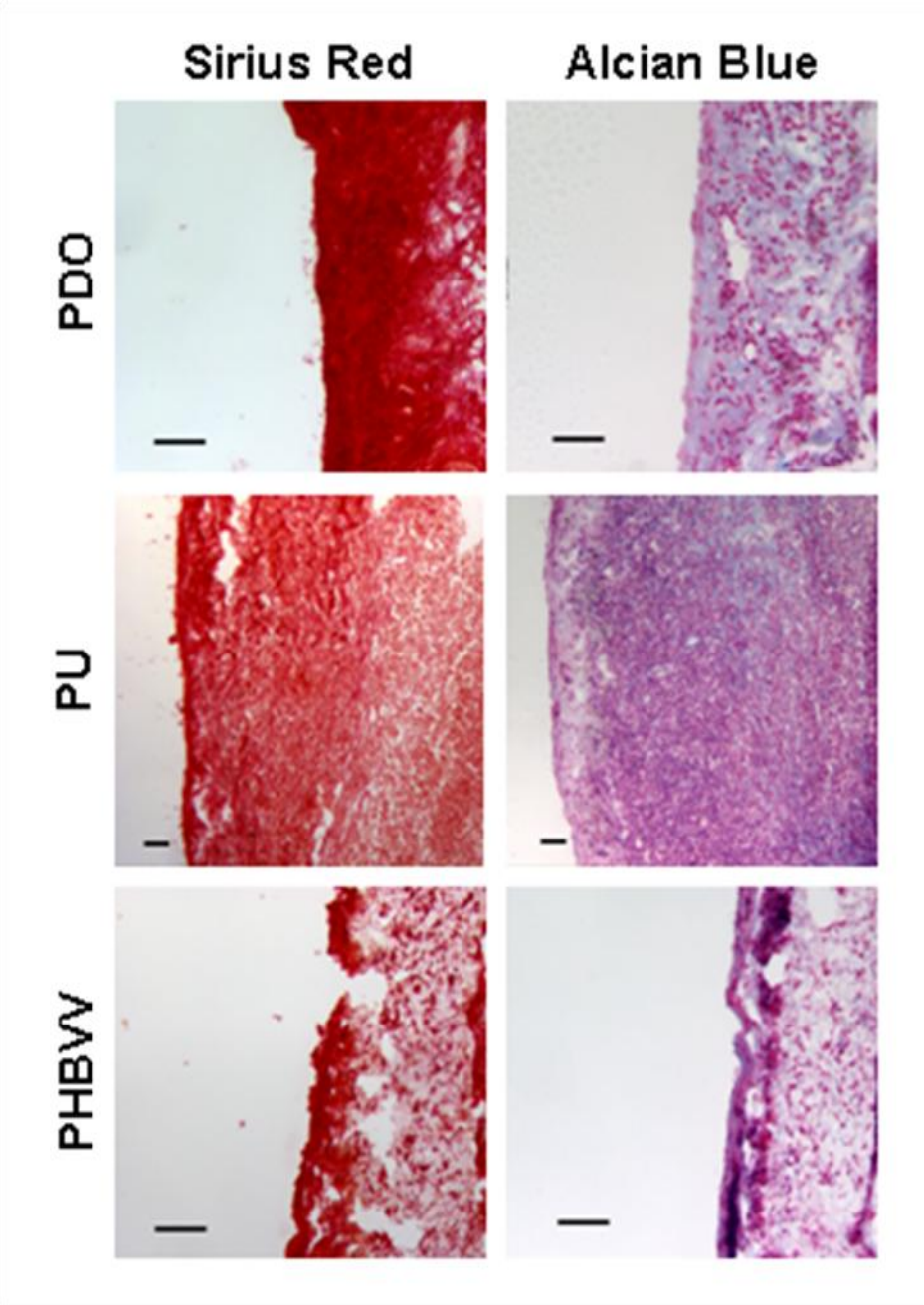

Figure 8. Extracellular matrix synthesis of the biopolymer patches explanted after 3 months. PDO is the polymer showing the most similarities with the native rat IVC in terms of collagen (a) and glycosaminoglycans (b) density, followed by PHBVV (e,f). Extra-cellular matrix in contact with the PU material appears less well organized (c,d).

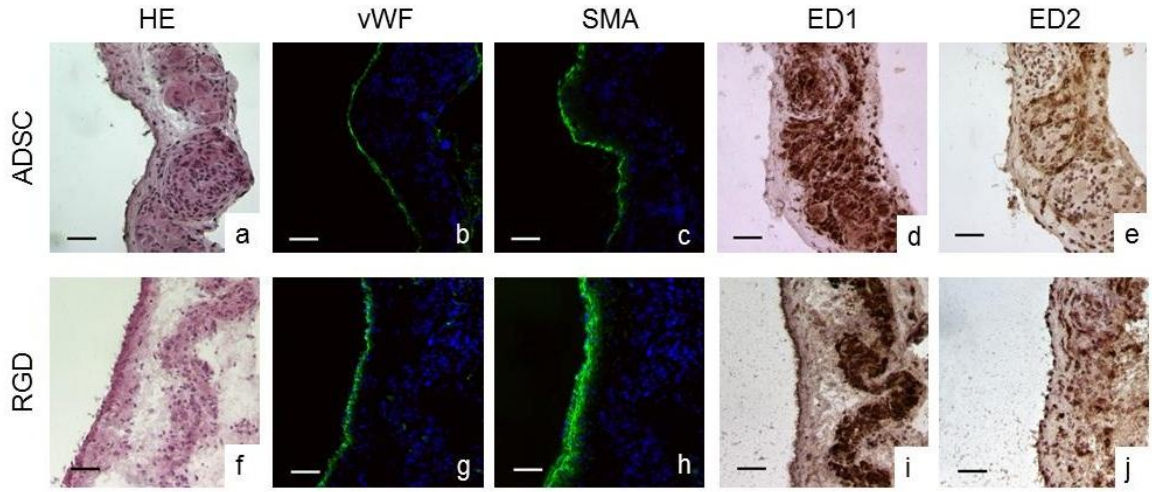

Figure 9. Analysis of the biofunctionalized patches removed after 6 weeks. Both ADSC and RGD-biofunctionalized patches are evenly lined with endothelial (b,g) and smooth muscle cells (c,h). ED1 (d,i) and ED2 (e,j) macrophages infiltrate both patches. Scale bar: 50 μm.

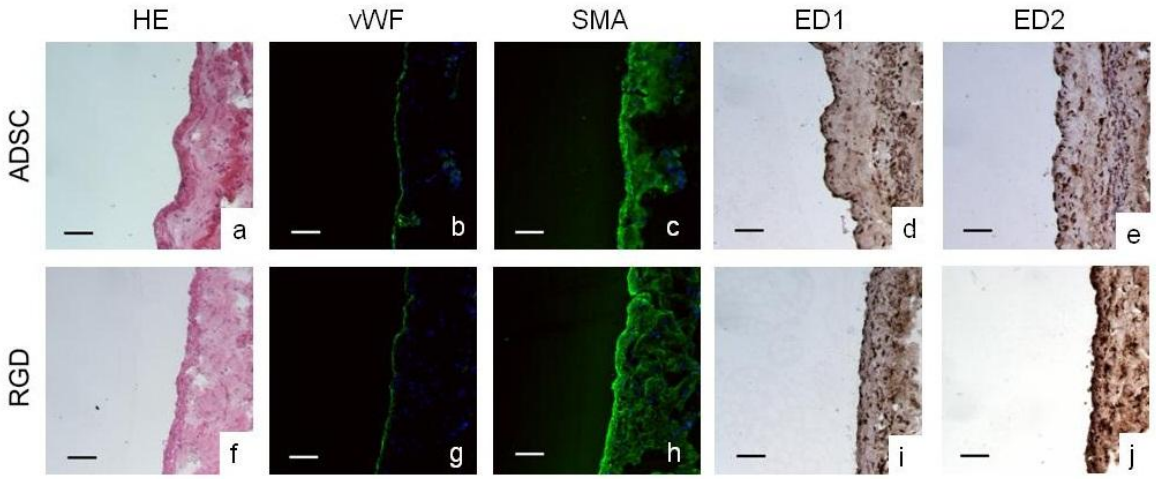

Figure 10. Analysis of the biofunctionalized patches removed after 3 months. Both ADSC and RGD-biofunctionalized patches are evenly lined with endothelial (b,g) and smooth muscle cells (c,h). Macrophage infiltration has distinctly decreased from 6 weeks, with a shift towards a regulatory pattern (e,j). Scale bar: 50 µm.

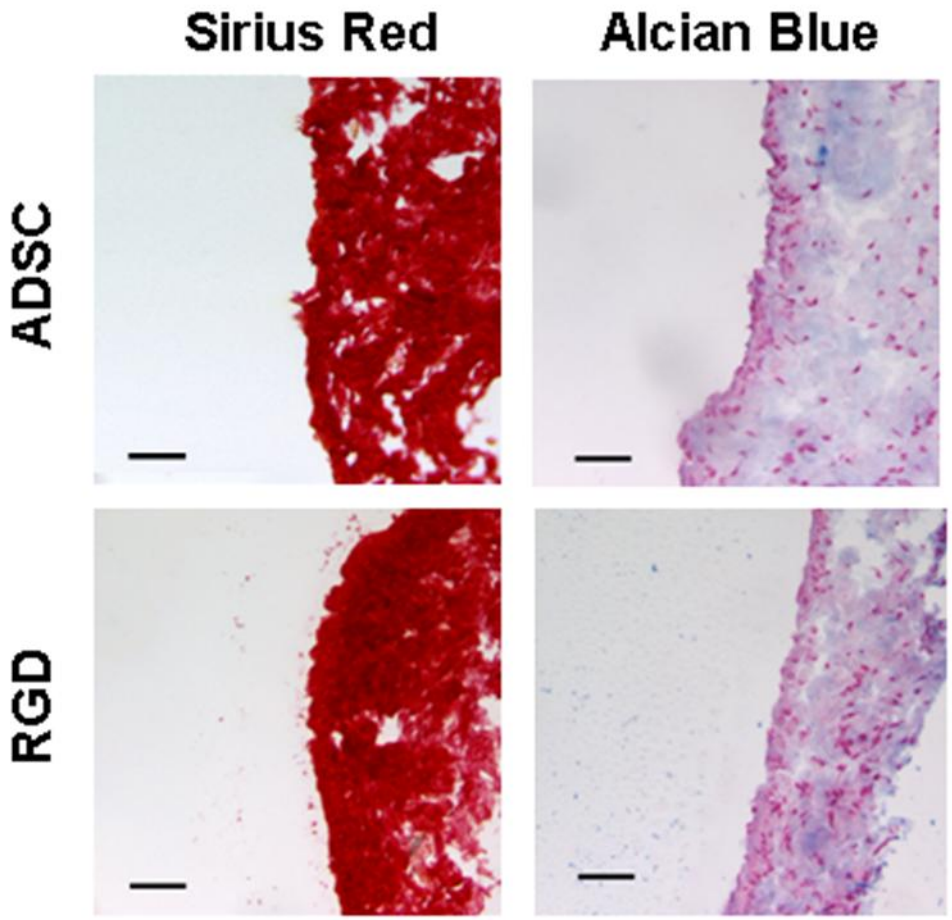

Figure 11. Extracellular matrix synthesis of the biofunctionalized patches explanted after 3 months. ADSC-seeded PDO (a,b) and RGD-grafted PDO (c,d) do not show any differences in extracellular matrix composition or organization, which are similar to those of the native IVC extracellular matrix.

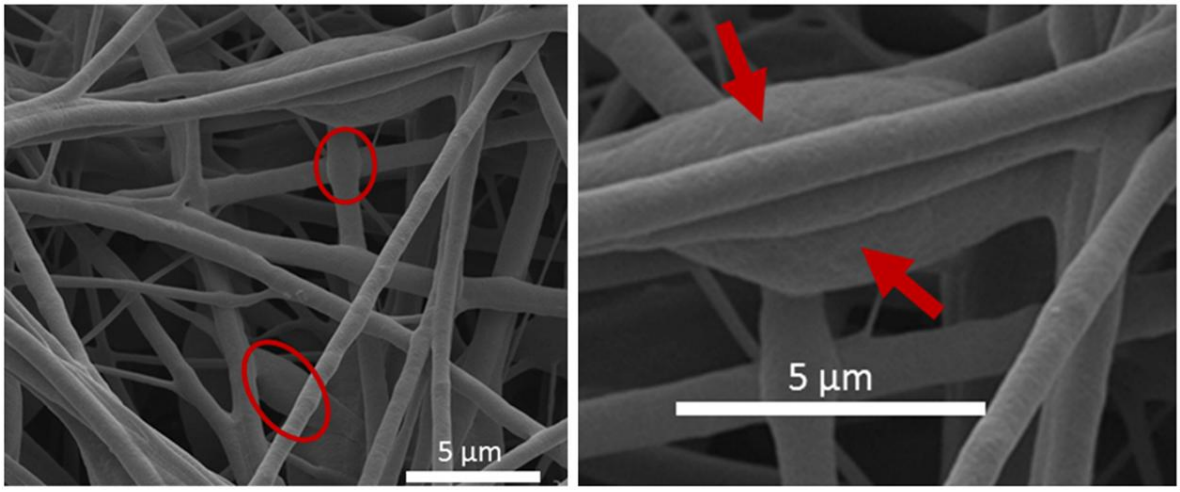

Supplemental figure 1. SEM images of the electrospun PHBVV fibre mats. Example of a bead on the string morphology of the PHBVV materials. It has not been included in the revised manuscript but could do based on the Editor's decision.

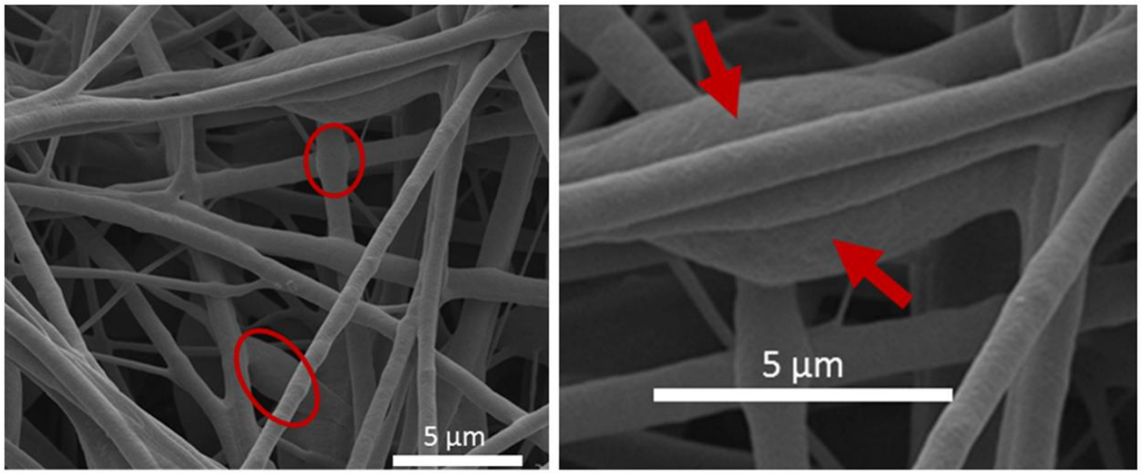

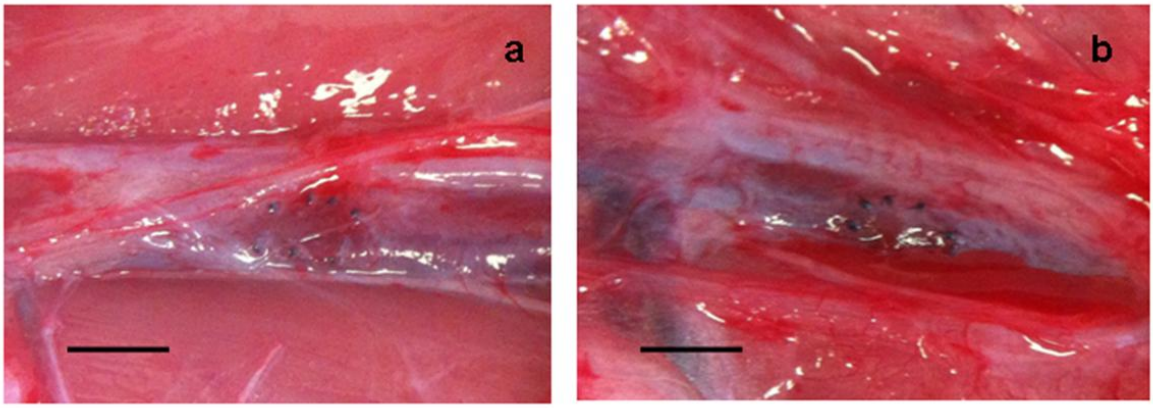

Supplementary figure 2 : Macroscopic views of the implanted biofunctionalized PDO patches (a : PDO and RGD ; b : PDO and ADSC). Biofuctionalized paches are integrated within the native IVC wall like bare PDO patches in the first set of biopolymer comparison (scale bar : 3mm).

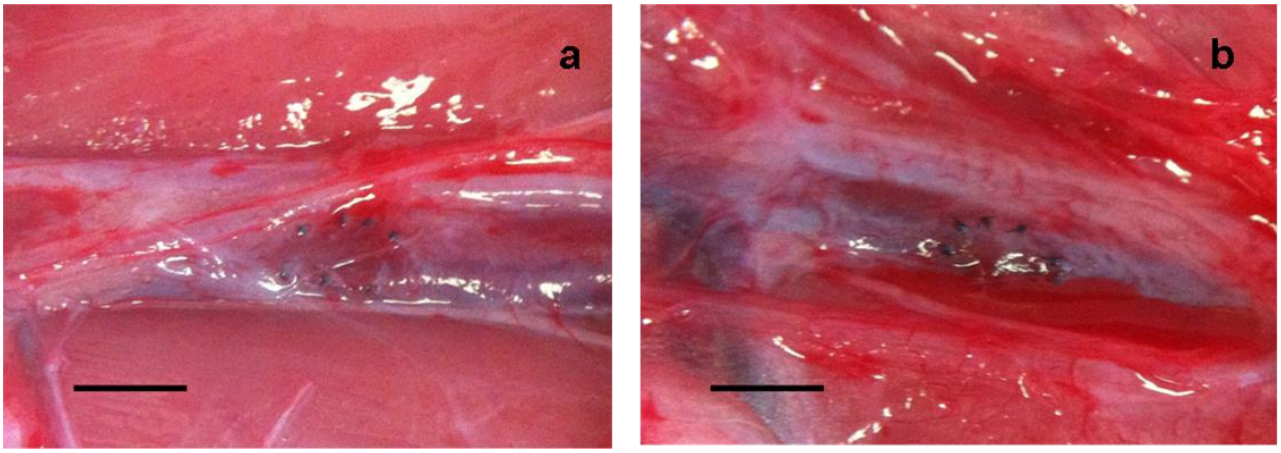

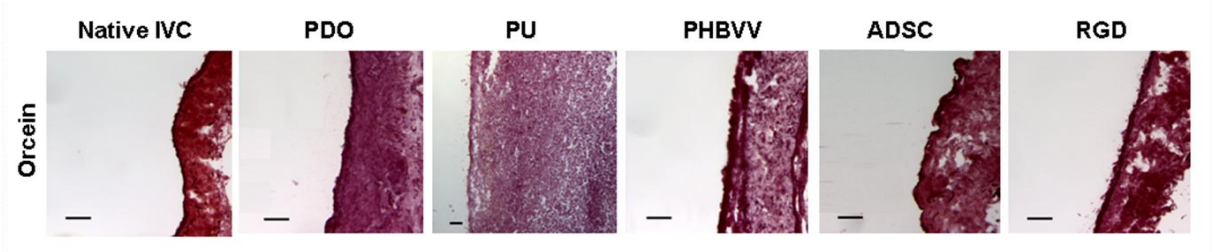

Supplemental figure 3. Orcein staining failed to detect elastic fibers in the ECM of the native IVC that were consequently equally absent in all polymer-treated groups.

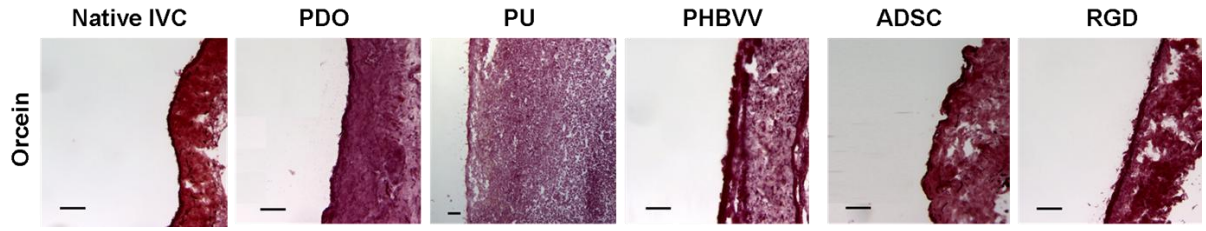

Table 1. The electrospinning parameters used to prepare patches of PDO, PU, and PHBVV.

Fibre ID	Polymer	Solvent	Polymer conc. (% w/v)	RGD conc. (mg/mL)	Applied voltage (kV)
PDO	PDO	HFIP	7	0	13.5
PU	PU	HFIP	5	0	15
PHBVV	PHBVV	Chloroform	7	0	12
PDO-RGD	PDO	HFIP	7	1.7	13.5

Table 2. Characterising data on the ES fibers produced. Diameters are reported as mean ± S.D., and porosity has been calculated using the method of Ghasemi-Mobarakeh et al (Ghasemi-Mobarakeh, L., Semnani, D. & Morshed, M. A novel method for porosity measurement of various surface layers of nanofibers mat using image analysis for tissue engineering applications. J. Appl. Polym. Sci. 106, 2536-2542 (2007).)

Fibre ID	Diameter (nm)	Porosity (%)
PDO	578 ± 234	85.3
PU	856 ± 198	88.5
PHBVV	606 ± 268	86.1
PDO-RGD	133 ± 28.1	84.5

Table 3. Histological and ELISA assessments of non-biofunctionalized polymers at 6 weeks. [Data were analyzed by analysis of variance or analysis of variance on ranks (when appropriate) for quantitative variables ; exact Fisher test for qualitative variables ; pairwise comparisons with Tukey correction for multiple comparisons ; ns : not significant]

	PDO (n=15)	PU (n=18)	PHBVV (n=11)	Global p-value
VWF (%)	100	100	100	ns
SMA (%)	96 (±9)	59 (±35)	89 (±22)	0.0006
ED1 (%)	92 (±14)	92 (±12)	71 (±24)	0.0038
ED2 (%)	50 (±13)	66 (±19)	37 (±17.5)	0.0002
ED2/ED1 (%)	55 (±14)	72.5 (±19)	58 (±30)	0.0414
Granuloma, n(%)	0	4 (22)	0	ns
IL 6 (pg/mL)	305 (±195)	163 (±143)	6 (±9.85)	<0.0001
MCP 1 (pg/mL)	25073 (±10736)	13009 (±7552)	5782 (±6491)	<0.0001
iNOS (ng/mL)	2.56 (±4.06)	2.58 (±2.88)	1.40 (±1.01)	ns
IL 10 (pg/mL)	2186 (±1279)	1309 (±1177)	807 (±613)	0.015

Table 4. Histological and ELISA assessments of non-biofunctionalized polymers at 3 months.

	PDO (n=3)	PU (n=3)	PHBVV (n=3)
VWF (%)	100	100	100
SMA (%)	100	78 (±29)	100
ED1 (%)	12 (±3)	83 (±6)	38 (±28)
ED2 (%)	12 (±3)	47 (±6)	20 (±9)
ED2/ED1 (%)	100	56 (±6)	64 (±31)
Granuloma	0	3 (100)	0
IL 6 (pg/mL)	433 (±64)	254 (±49)	12 (±9,6)
MCP 1 (pg/mL)	14998 (±6915)	11170 (±2381)	4800 (±5732)
iNOS (ng/mL)	1.52 (±0.95)	2.73 (±1.04)	2.74 (±2.45)
IL 10 (pg/mL)	2117 (±305)	1228 (±307)	1567 (±805)

Table 5. Histological and ELISA assessments of biofunctionalized polymers at 6 weeks. (Data were analyzed by Student and Wilcoxon Mann-Whitney tests ; ns : not significant.)

	ADSC (n=10)	RGD (n=7)	p-value
VWF (%)	100	100	ns
SMA (%)	97 (±5)	100	ns
ED1 (%)	100	93 (±9.5)	0.049
ED2 (%)	36.5 (±12)	43 (±18)	ns
ED2/ED1 (%)	36.5 (±12)	47 (±19)	ns
IL 6 (pg/mL)	16 (±25)	12 (±19)	ns
MCP 1 (pg/mL)	7112 (±9548)	3949 (±6920)	ns
iNOS (ng/mL)	0.67 (±0,40)	0.65 (±0.51)	ns
IL 10 (pg/mL)	1197 (±938)	1088 (±1490)	ns

Table 6. Histological and ELISA assessments of biofunctionalized polymers at 3 months. (Data were analyzed by Student and Wilcoxon Mann-Whitney tests ; ns : not significant)

	ADSC (n=7)	RGD (n=7)	p-value

VWF (%)	100	100	ns
SMA (%)	100	100	ns
ED1 (%)	66 (±39)	69 (±25)	ns
ED2 (%)	41 (±30)	51 (±23)	ns
ED2/ED1 (%)	69 (±31)	76 (±21)	ns
IL 6 (pg/mL)	31 (±25)	18 (±19)	ns
MCP 1 (pg/mL)	17594 (±13235)	6574 (±5751)	ns
iNOS (ng/mL)	1.31 (±0,93)	2.79 (±2.86)	ns
IL 10 (pg/mL)	1392 (±645)	1266 (±637)	ns